Journal of Petroleum Science and Technology 13(2): 38, 2023, Pages 29-39
DOI:10.22078/jpst.2023.5017.1852

Journal of Petroleum Science and Technology

Research Paper

https://jpst.ripi.ir/

Wellbore Optimum Stability of Oil Well Drilled in a Highly Fractured Carbonate Reservoir Based on Dipole Sonic Analysis

Ehsan Saadatzadeh*, Khalil Shahbazi and Reza Salehi
Faculty of Petroleum, Petroleum University of Technology, Ahwaz, Iran

Abstract

Wellbore stability is dominated by in-situ stress and geomechanical parameters of formation rocks, so estimating these parameters around the wellbore is important. The studied well is a suitable candidate for investigation of wellbore stability due to continuing directional drilling and planning for oriented perforation and hydraulic fracturing program from the wellbore and availability of dipole sonic, nuclear magnetic resonance (NMR), core image, and log data to optimize and estimate wellbore stability conditions. In this study, the rock permeability is derived from dipole sonic analysis to investigate the certainty of the model; these results are compared with NMR and special core analysis results. Then, based on these results, pore pressure, in-situ stress, rock mechanical properties, stress and fracture distributions, and anisotropy of formation are calculated and compared with Image log Results. Finally, the optimum mud weight to avoid wellbore failure can be estimated from all these data. As the final results, the maximum horizontal stress direction is N33E, and most open fractures are in this direction. The minimum horizontal stress direction is in N57W, and the safe and appropriate mud weight is between 6.5 and 7.5 ppg, which can be considered 7 ppg. This technique is based on dipole sonic analysis that can be applied to investigate wellbore stability in intervals with no core or image log analysis.

Keywords: Wellbore Stability, In-situ Stress, Dipole Sonic, Fracture Distributions, Anisotropy, Mud Weight.

Introduction

More than 60% of the world's oil and 40% of the world's gas reserves are in carbonate reservoirs [1]. In these reservoirs, a combination of depositional fabrics, diagenetic alterations, and fracturing controls the reservoir quality [2]. A natural fracture system in the rock can often be found near faults. Rock near faults can be broken into large or small pieces. If they are loose, they can fall into the wellbore and jam the string in the hole [3]. Accordingly, fractures and wellbore collapse are two kinds of wellbore instability problems [4].

On the other hand, wellbore fracture happens when the mud weight is larger than the fracture pressure. The wellbore is in tension condition, and wellbore collapse happens when mud weight in the wellbore does not support external pressure [5]. Detailed wellbore stability analysis needs a complete dataset, including core and petrophysical data, which are not always available [6]. Unexpected or unknown behavior of rock is often the cause of drilling problems, resulting in an expensive loss of time, sometimes in a loss of part or even whole borehole [7, 8]. Rock formation remains stable and in equilibrium condition before drilling. After drilling, there is a disturbance that changes the stability condition. Wellbore stability is dominated by the in-situ stress system. When drilling a wellbore, the rock surrounding the wellbore must take the load previously taken by the removed rock. As a result, the in-situ stress changes in the borehole wall. This stress can lead to rock failure. This problem can be avoided by adjusting the mud weight. So that stress concentration around the borehole wall can be managed to minimize borehole failure [9]. The unconfined compressive strength (UCS) of sedimentary rocks is a key parameter needed to address a range of geomechanical problems ranging from limiting wellbore instabilities during drilling [10] to assessing sanding potential [11] and quantitatively constraining stress magnitudes using observations of wellbore failure [12]. Borehole stability is a continuing problem that results in substantial yearly expenditures by the petroleum industry [13, 14]. Wellbore stability predictive models may also be used to design appropriate completions for inflow problems where hole collapse and associated sand production, or even the complete loss of the well, may

**Corresponding author:* Ehsan Saadatzadeh, Petroleum University of Technology, Ahwaz, Iran
E-mail addresses: ehsansaadatzadeh@gmail.com
Received 2023-01-23, Received in revised form 2023-12-06, Accepted 2023-12-24, Available online 2024-02-12

be concerned [15]. Recognizing stress direction is very important in the exploration and production of oil. It is effective in wellbore stability, flow unit patterns, fluid flow in fractured reservoirs, cap rock failure, and fault reactivation [16]. Natural fractures that are parallel to the Maximum Horizontal Stress (Shmax) - (or oblique to that) are capable of tensile or shear deformation, and mostly observed that these types of fractures are more permeable (open fractures) [17].

Most of Iran's oil-producing horizons are related to the Oligocene–Miocene Asmari Formation [18, 19]. Due to a lack of necessary data, the role of geomechanic parameters is still unknown in most Iranian reservoirs [20]. For the current study, an exceptionally comprehensive dataset (Cores, Image log, Dipole Sonic log, and Conventional Logs) in oil well enabled us to characterize various geomechanical parameters, petrophysical aspects of rock mechanic parameters, delineate their effect on reservoir anisotropy and investigate mud weight window as an important factor in wellbore stability in the Asmari Formation of a supergiant highly fractured oilfield of southwestern Iran. The studied well location in this reservoir is represented in Fig. 1.

Materials and Methods

In this study, as a first step, the rock permeability is derived from dipole sonic analysis by slowness-time coherency (STC) technique and flow zone indicator (FZI) model, and for investigating the certainty of the model, these results are compared with nuclear magnetic resonance (NMR) and special core analysis (SCAL) permeability results. Then, based on these results, pore pressure, in-situ stress, rock mechanical properties, stress and fracture distributions, and anisotropy of formation are calculated. Afterwards, the anisotropy, stress, and fracture distributions are compared with Image log results. Finally, the optimum mud weight to avoid wellbore failure can be estimated from all these data. By generating mud-safe windows, problems related to wellbore instability during drilling can be avoided. The schematic of the overall work is represented in Fig. 2.

Dipole Sonic Imager Tool

Dipole Sonic Imager Log (DSI) is a modern sonic log that makes compressional, shear, and stoneley waves to recognize the petrophysical and geomechanical properties of the rocks. The schematic and specification of this tool are presented in Fig. 3.

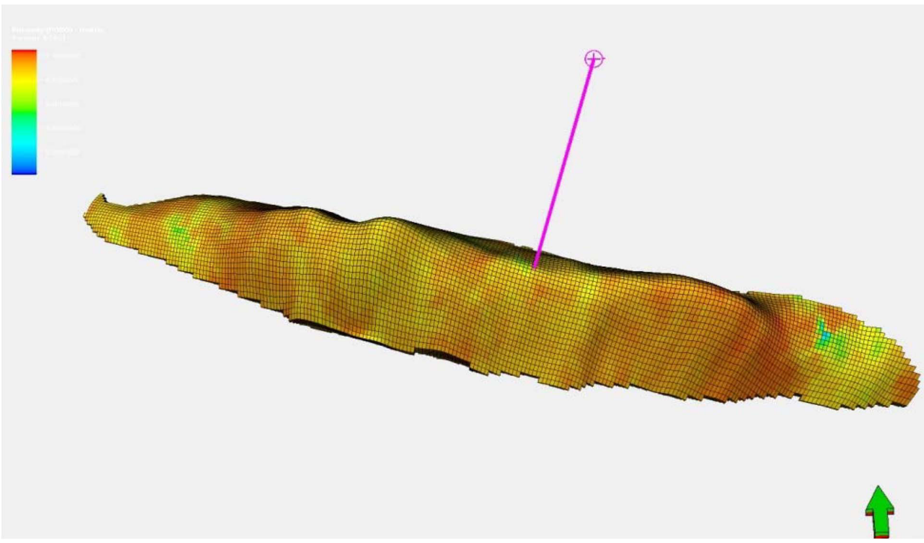

Fig.1 Well Location in Reservoir.

Fig. 2 Schematic of Overall Work of Study.

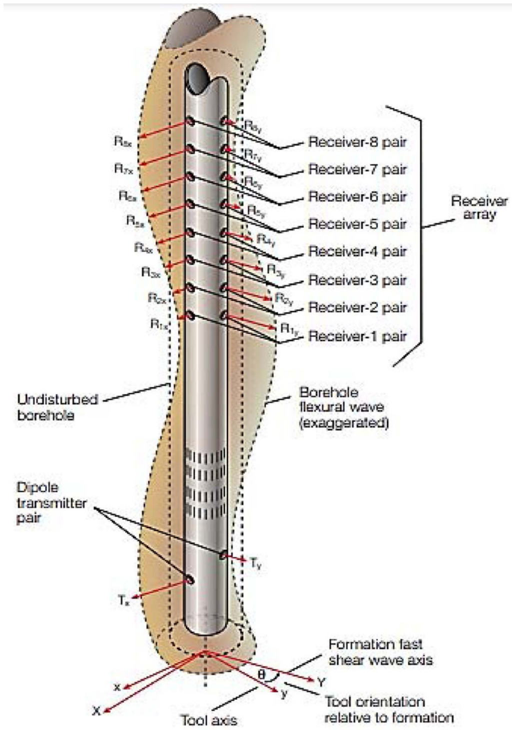

Fig. 3 Schematic and Specification of DSI Tool.

Permeability Derivation from Dipole Sonic Log

Considering the clearness of the distance between the receivers of the DSI tool and the linear slope obtained from the connection of similar components in different receivers, the velocity of that component is calculated. The higher the slope of this line, the higher the velocity of the sonic wave and the lower its slowness. Therefore, naturally, compressional wave (P-Wave) slowness will be less than shear wave (S-Wave), and shear wave slowness will be less than stoneley wave [21, 22]. Using the mathematical technique of similarity analysis (Semblance), all waveforms received in different receivers, using a moving time window, are scanned until similar arrival times, based on the degree of coherence, are separated. All types of sonic waves (P, S, and Stoneley) are distinguished in the monopole mode. Slowness Time Coherency (STC) is obtained by plotting the slowness calculated from the similarity analysis regarding arrival time. By connecting the STC of different depths, it is possible to derive the attenuation of different components of the sonic wave. Stoneley waves in low frequencies are propagated inside the wellbore like a tube wave. When the Stoneley wave passes through the permeable portion or fracture, some of the wave's energy is reduced, resulting in wave attenuation and an increase in its slowness value. Fractures and permeable areas have different effects on the Stoneley wave.

It should be noted that the parameter measured with the Stoneley wave indicates the ability of the fluid to move inside the formation (Stoneley Permeability). Among the factors affecting the slowing down of the Stoneley wave propagated inside the formation,the effect of the mudcake in front of the permeable zone, and the properties of the fluid inside the formation are important. In the FZI model, it is possible to estimate the permeability from Stoneley waves by relations 1 to 5:

$$Dt_{stCalc} = \sqrt{Dt_f{}^2 + \frac{\rho \times Dt_s h^2}{Rhob}} \quad (1)$$

$$K_{ist} = \frac{Dt_{st\,DSI}}{Dt_{st\,Calc}} \quad (2)$$

$$IMF = \sum^{(IMF_i \times V_i)} \quad (3)$$

$$FZI = IMF \times (K_{ist} - 1) \quad (4)$$

$$K_{st} = 1014 \times FZI^2 \times [\frac{\phi_e^3}{(1-\phi_e)^2}] \quad (5)$$

where $Dt_{st\,Calc}$, Dt_f, Dt_{sh}, $Dt_{st\,DSI}$, ρ_f, Rhob, K_{ist}, IMF, V_i, FZI, ϕ_e and K_{st} are stoneley slowness, mud filtrate slowness, shear slowness, DSI stoneley slowness, mud filtrate density, bulk density, permeability index, index match factor, mineral volume, mineral, flow zone indicator, effective porosity, and stoneley permeability, respectively [23].

Geomechanical Parameters Estimation

The compressional slowness (DTC) and shear slowness (DTSh) obtained from the DSI were combined with the bulk density to compute the dynamic elastic moduli. The following dynamic elastic moduli can be computed using the DSI formation density data [24, 9]:

$$Dynamic\ Shear\ Modulus = G_{Dyn} = (92903.04)\frac{RHOB}{Dt_s h^2} \quad (6)$$

$$Dynamic\ Bulk\ Modulus = K_{Dyn} = (92903.04) RHOB \frac{1}{Dt_c^2} - \frac{4}{3} G_{Dyn} \quad (7)$$

$$\text{Dynamic Young's Modulus} = E_{Dyn} = 2\, G_{Dyn}\, (1+v) \quad (8)$$

$$Dynamic\ Poisson's\ Ratio = V_{Dyn} = \frac{0.5(Dt_s h / Dt_c)^2 - 1}{(Dt_s h / Dt_c)^2 - 1} \quad (9)$$

$$\text{Static Young's Modulus} = E_{sta} = (-2.21\,\phi_e + 0.963) E_{Dyn} \quad (10)$$

The static Young's modulus was used to get the static Unconfined Compressive Strength (UCS) profiles. For all the formations, the following correlation has been used [25, 6]:

$$UCS = (4.1 E_{sta} + 3) 145 \quad (psi) \quad (11)$$

The tensile strength is obtained from the UCS by dividing it by a certain number. Generally, this number varies between one-tenth and one-twelfth of the UCS. The Asmari Formation in this study was taken as one-tenth of the UCS computed by the Young's modulus correlation [26].

$$T_0 = \frac{UCS}{10} \quad (11)$$

Anisotropy Investigation

In deviatoric stress conditions, fractures that are parallel to SHmax remain open, and fractures perpendicular to SHmax will be closed. In this medium, a fast shear wave moves to the open fractures' direction (SHmax direction), and a slow shear wave moves to the closed fractures' direction (SHmax direction) [10, 27]. Fast shear wave direction can be determined as an AZIM-FAST curve showing higher rock compaction direction (Fig. 4). This curve shows the direction in which the rock is denser, and in this way, the direction of the maximum horizontal stress (SHmax) can be determined at all depths. Since the Breakouts in the shear waves are in the direction of minimum horizontal stress (Shmin), as the anisotropy direction of achieved raw data is not parallel with the formation anisotropy direction, the axis of the tools can be paralleled with the formation anisotropy direction [8, 28].

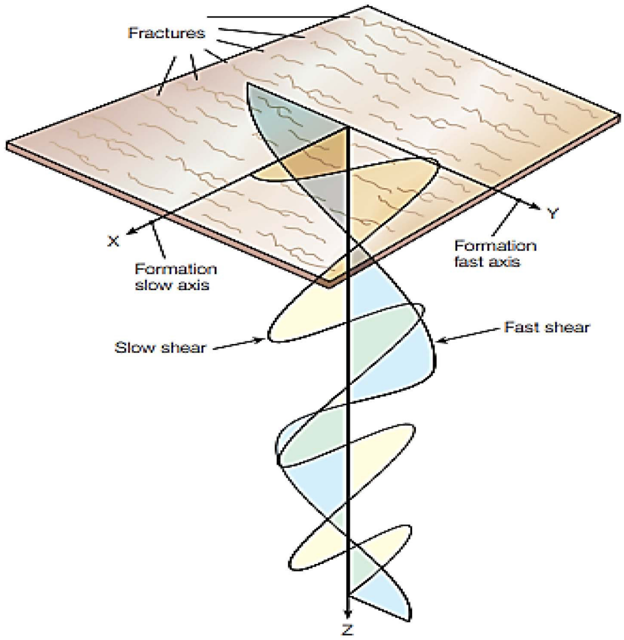

Fig. 4 Shear Waves Splitting in the Presence of Fractures.

By calculating the anisotropy, two curves showing the minimum and maximum energy (MIN and MAX- ENERGY) are finally obtained. In the isotropic depth interval, the values of energy anisotropy are zero, and in the anisotropic depth interval, the reading value depends on the intensity of anisotropy. Also, anisotropy is compared with oil-based mud-ultrasonic borehole Imager log (OBMI-UBI) anisotropy to check the model certainty.

To calculate the horizontal minimum and maximum stresses based on the isotropic poroelastic horizontal strain model:

$$SHmax = v_{Dyn} * \frac{P_{ob} - \alpha * P_{for}}{1 - v_{Dyn}} + \alpha * P_{for} + \frac{E_{Dyn} * e_{max}}{1 -^{2}_{Dyn}} + \frac{v_{Dyn} * E_{Dyn} * e_{min}}{1 -^{2}_{D} yn} \quad (13)$$

$$SHmin = _{Dyn} * \frac{P_{ob} - * \alpha P_{for}}{1 - v_{D} yn} + \alpha * P_{for} + \frac{E_{Dyn} * e_{min}}{1 -^{2}_{Dyn}} + \frac{v_{Dyn} * E_{Dyn} * e_{max}}{1 -^{2}_{D} yn} \quad (14)$$

e_{min} and e_{max} are empirical constants which define the tectonic strain in the minimum and maximum horizontal stress directions. Interpretation of mini-frac tests can be used to adjust the minimum horizontal stress. Borehole failure, such as breakout and tensile fractures observed on image logs, can be used to calibrate the maximum horizontal stress. Pob, Pfor, and α are overburden pressure, formation pressure, and Biot factor. Pob is calculated by integrating bulk density log values (RHOB) versus depth for offshore and onshore cases. Also, from the ratio of the formation pressure to the overburden stress, a linear gradient is derived between two pressure points. The interpolated formation pressure value is the product of the overburden and the gradient at the current depth. The biot factor is assumed to have an average value of 0.7 [23, 29].

Wellbore Stability Calculations

To analyze the wellbore's stability, the rock's mechanical properties and the rock stresses must be estimated. Various parameters affect wellbore stability, and the most important controllable parameter is the weight of the drilling mud. The suitable window for drilling fluid weight is determined after determining the mechanical properties of the rock, pore pressure, and rock stresses near the wellbore. The Coulomb failure criterion is used in this model to determine if the shear stress is sufficient enough to overcome the resistance to sliding. To be able to run this analysis, the formation pressure (P_{for}), the magnitudes of the three principal stresses (P_{ob}, SH_{min}, SHmax), and the orientation of SH_{max} (AZIM_SH_{max}) must be known. Fracture data from a borehole image log should be in a dip set. The results should be written into the same dip set [30].

Results and Discussion

Applying STC analysis, the compressional, shear, and stoneley waves are derived from the dipole sonic log (Fig. 5). The results of stoneley permeability by the FZI model and its comparison with core permeability through SCAL are represented in Fig. 6.

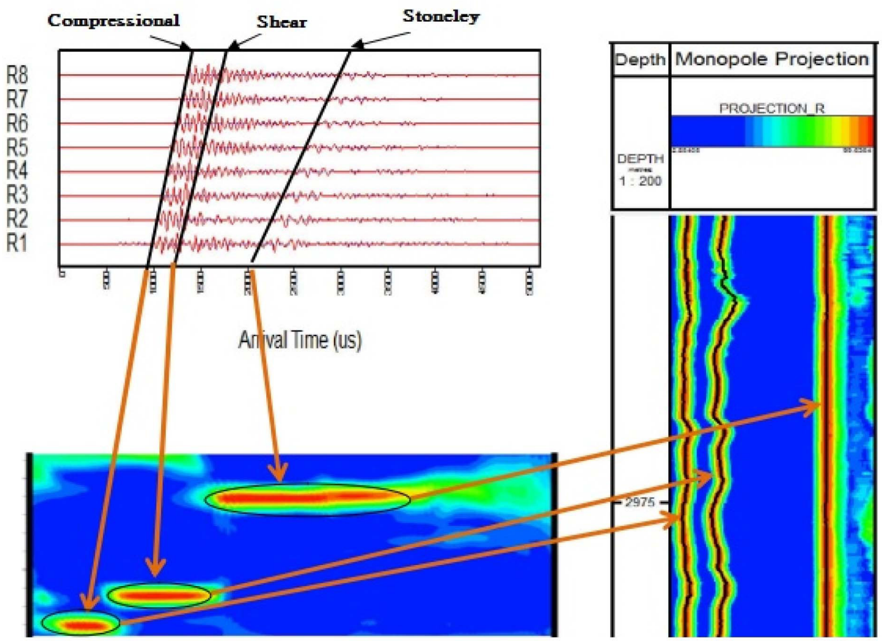

Fig. 5 STC Analysis Results for Compressional, Shear and Stoneley Waves Derivation.

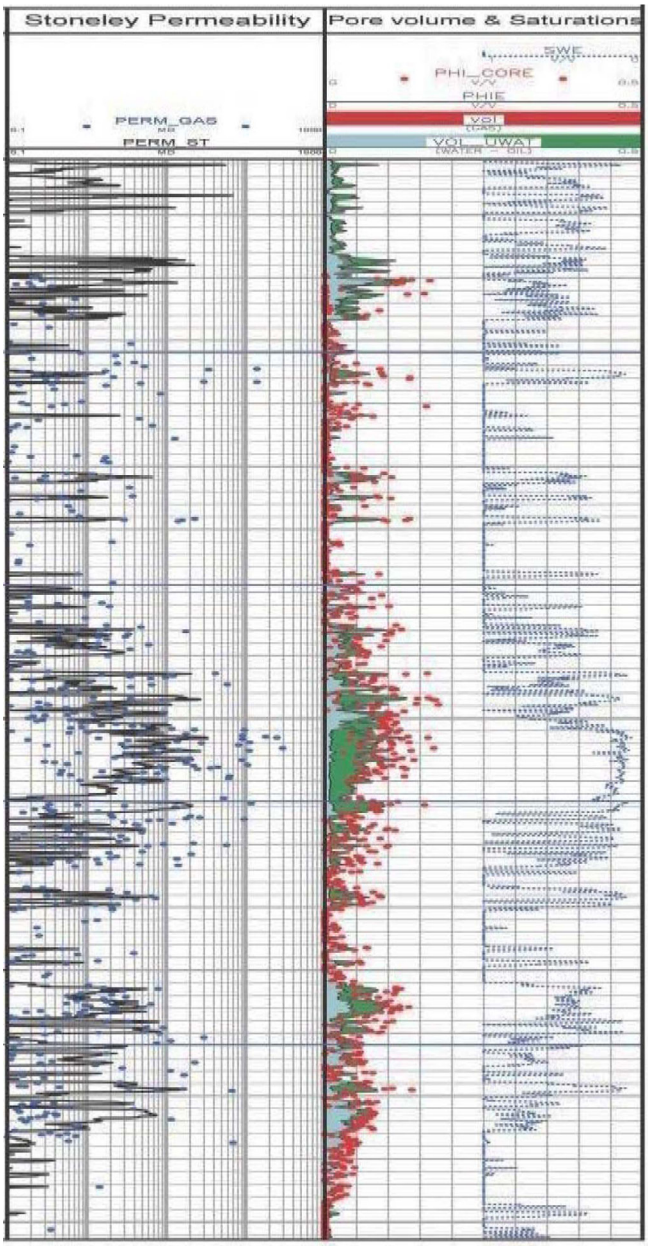

Fig. 6 Stoneley Permeability from FZI Model and Its Comparison with SCAL.

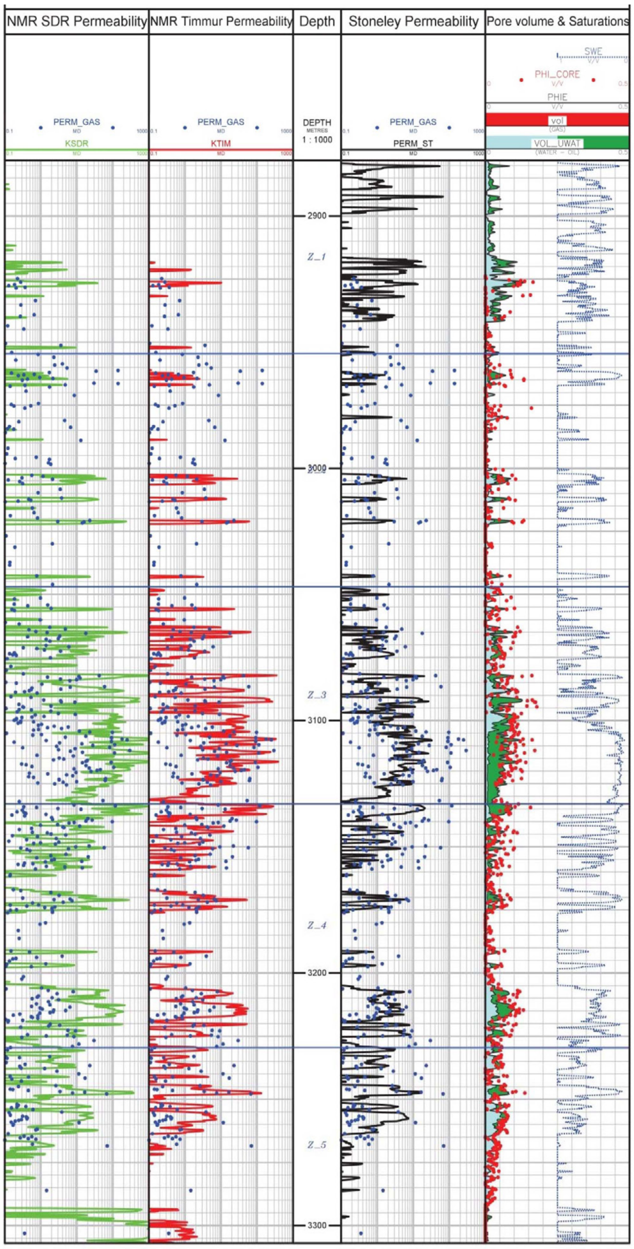

Fig. 7 Comparison of Stoneley Permeability with SCAL and NMR Results.

Comparison of calculated permeability results with NMR log permeability through two models (Timmur-Coats and SDR) are represented in Fig. 7 and summarized in Table 1. A good match of sonic results with SCAL and NMR confirms model certainty and can be applied to a geomechanical study.

Geomechanical moduli of formation rock are estimated from the sonic wave, and their changes in the whole depth interval of the wellbore are represented in Fig. 8.

Unconfined Compressive Strength (UCS) profile versus static Young's modulus that indicates the effective porosity changes in carbonate formation in well interval is represented in Fig. 9. The Polygon of calculated stresses is represented in Figure 10, indicating the wellbore stress trend. Anisotropy results rising from DSI and their comparison with OBMI-UBI results are presented in Fig. 11. According to this figure, the difference between Min and MAX-ENERGY is the anisotropy intervals matched with the image log. Also, AZIM-FAST shows the direction of maximum horizontal stress (SHmax), and breakouts represent the minimum horizontal stress (SHmin) direction.

Table 1 Summary of Permeability Results.

Layer	Interval (Meter)	SCAL Perm (mD)	SDR Perm (mD)	Timmur-Coats Perm (mD)	Stoneley Perm (mD)
Zone 1	2875-2950	1.559	1.81	1.82	1.71
Zone 2	2950-3045	0.472	0.25	0.26	0.16
Zone 3	3045-3125	2. 930	2.98	3.13	3.30
Zone 4	3125-3230	1. 391	1.15	1. 11	1.29
Zone 5	3230-3305	0.753	0.81	0.83	0.88

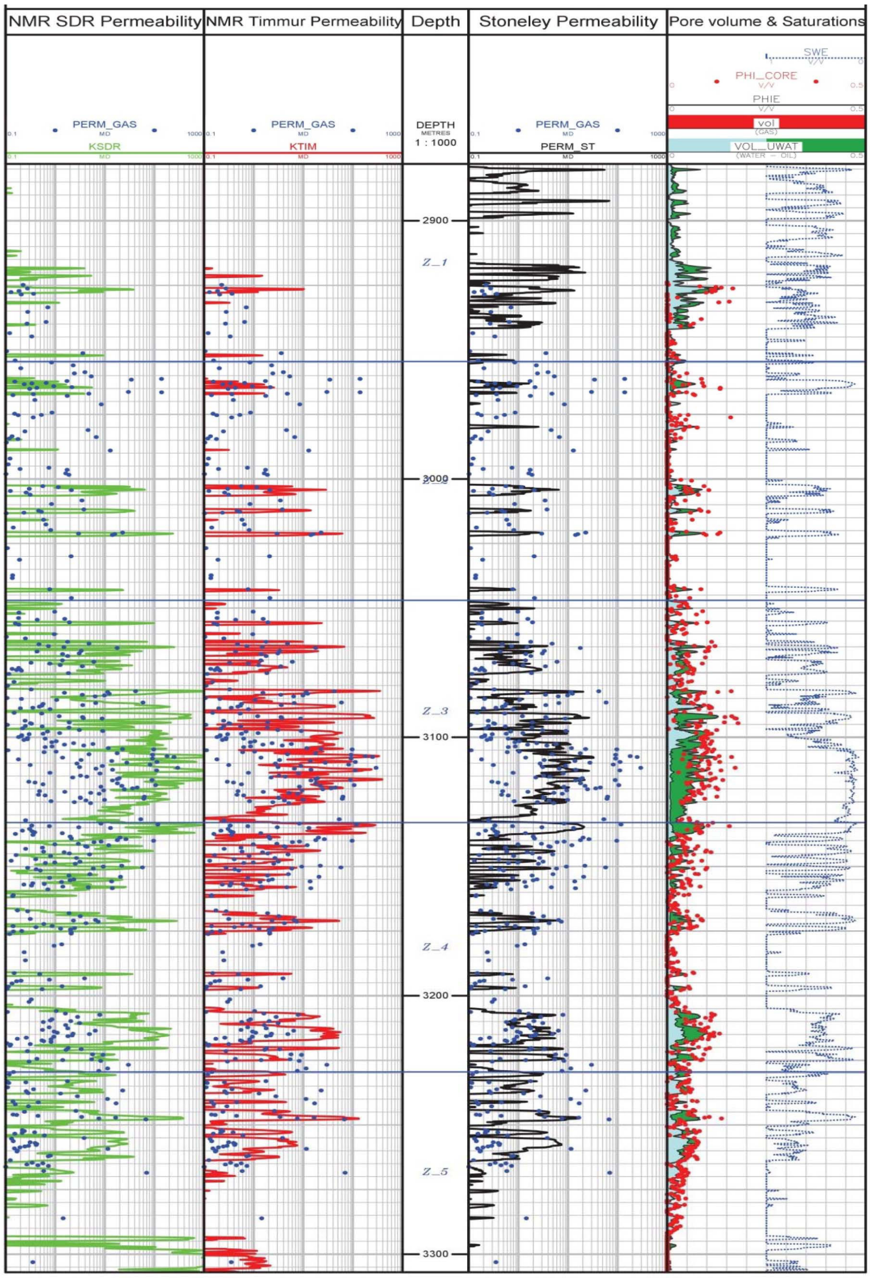

Fig. 8 Geomechanical Moduli for Whole Interval.

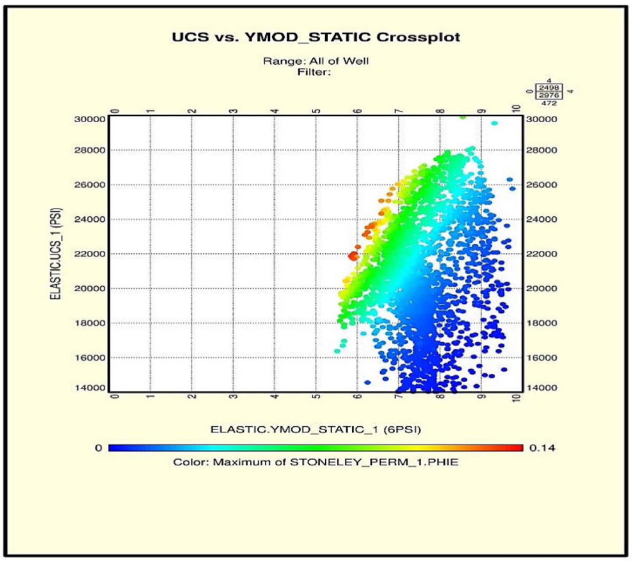

Fig. 9 UCS vs. Static Young's Modulus (Changing Color is Effective Porosity).

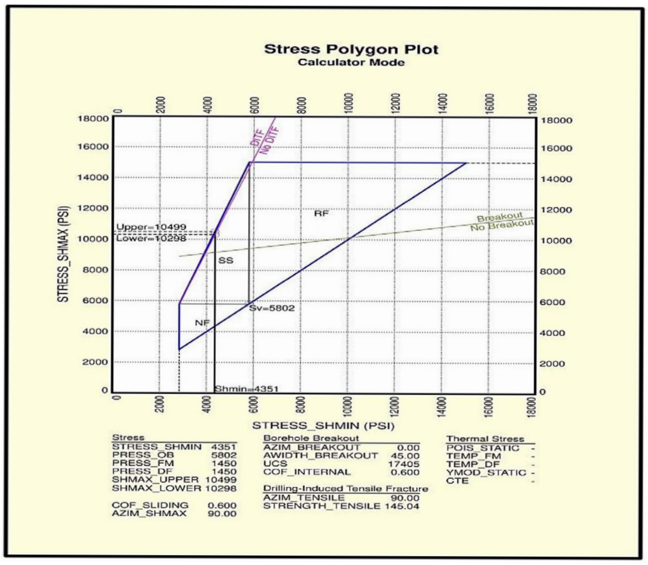

Fig. 10 Stress Trend in Depth Interval.

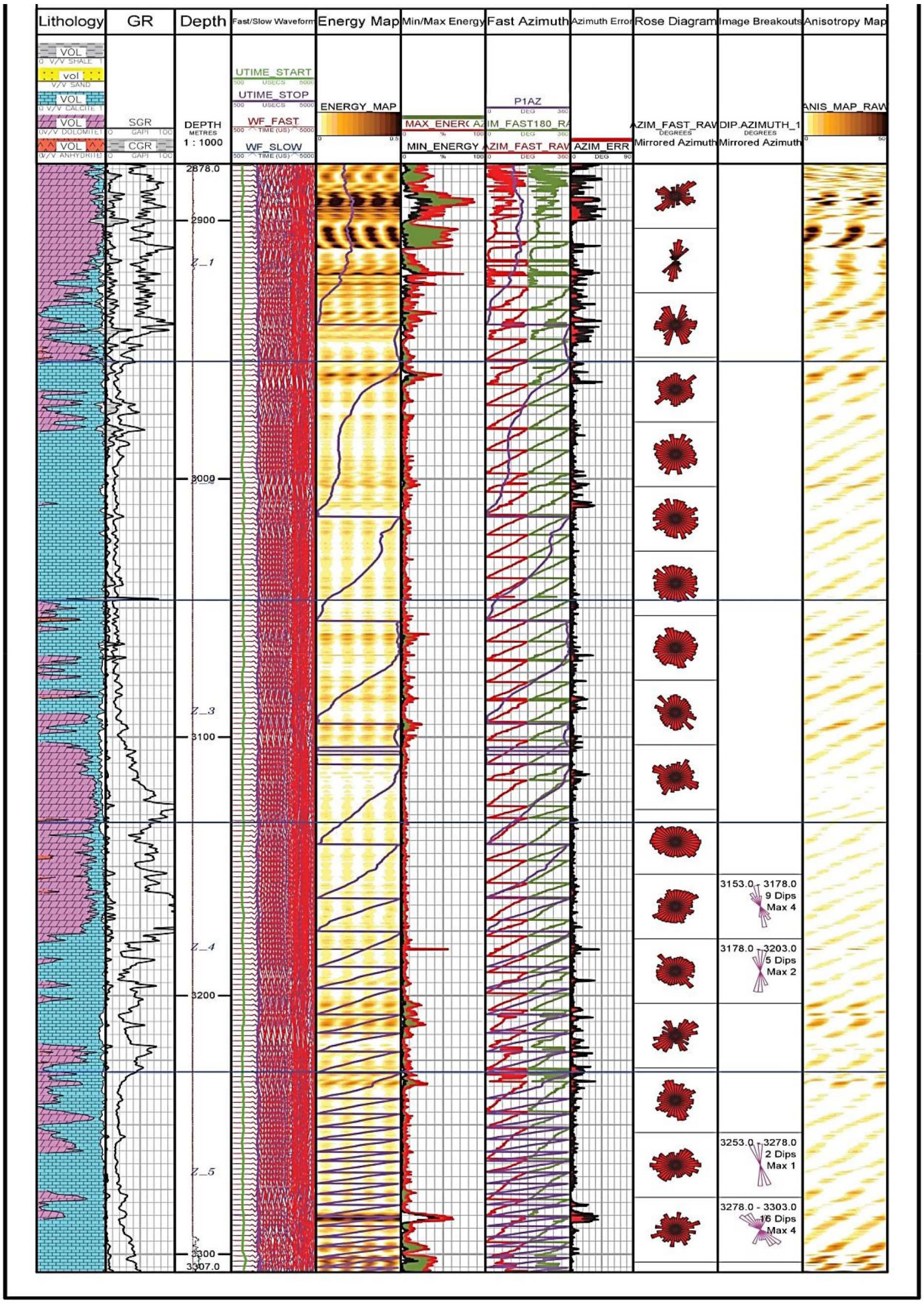

Fig. 11 Anisotropy Results (DSI and UBI Comparison).

Then, a wellbore walkout plot by applying dip and azimuth of bedding and fractures is prepared (Fig. 12), and based on this plot, wellbore stress is plotted according to maximum and minimum horizontal stresses (Fig. 13) to distinguish the tensile failures and breakout failures of overall depth interval. Also, the rose diagram of bedding and fractures that represents the maximum horizontal stress direction is plotted in Fig. 14.

A stereonet plot of wellbore stability based on rock strength is presented in Fig. 15. Also, a stereonet plot of wellbore stability based on mud weight is presented in Fig. 16. In these figures, the direction of SHmax is shown. SHmax direction is calculated as N33E.

The calculated pressures based on rock and drilling fluid geomechanical parameters transform to equivalent mud weight. The appropriate mud weight range for safe drilling is presented as a mud weight window in Fig. 17. In this figure, safe drilling is considered between fluid kick and formation breakout by mud, and based on this graph, the safe mud weight is between 6.5 and 7.5 ppg.

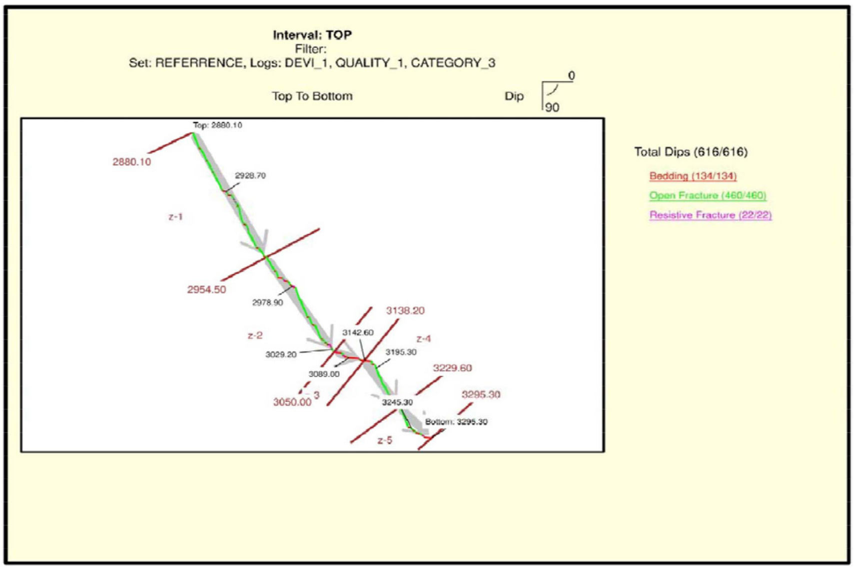

Fig. 12 Wellbore Walkout Plot based on Bedding and Fractures Dip and Azimuth.

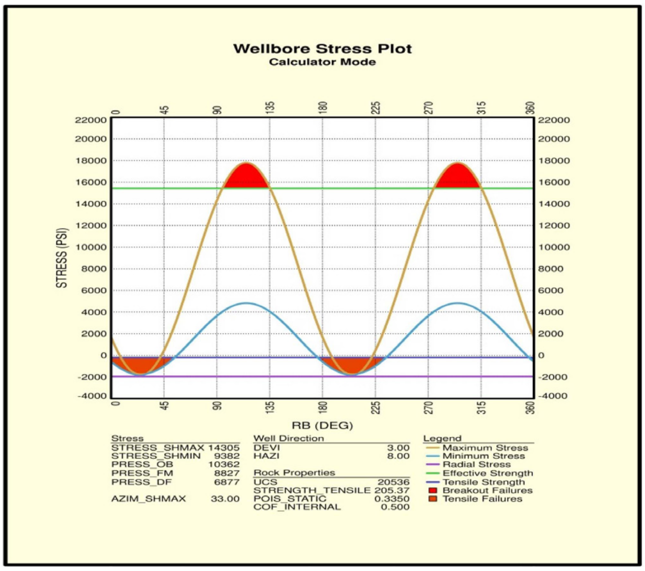

Fig. 13 Wellbore Stresses in Overall Interval.

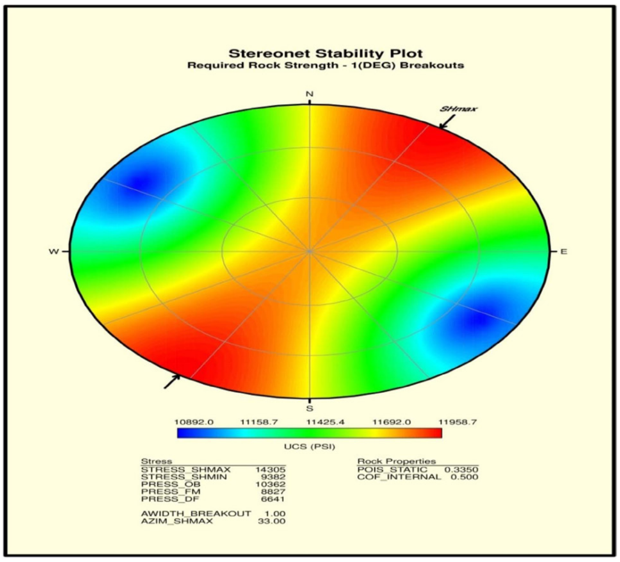

Fig. 15 Stereonet of Wellbore Stability Based on Rock Strength.

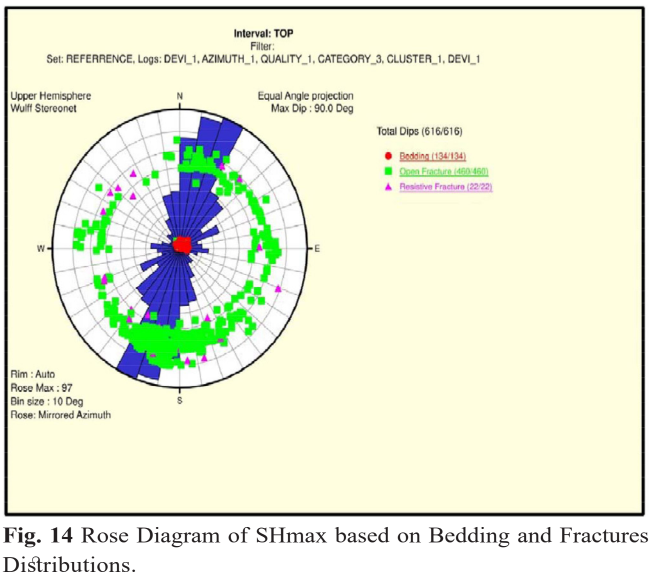

Fig. 14 Rose Diagram of SHmax based on Bedding and Fractures Distributions.

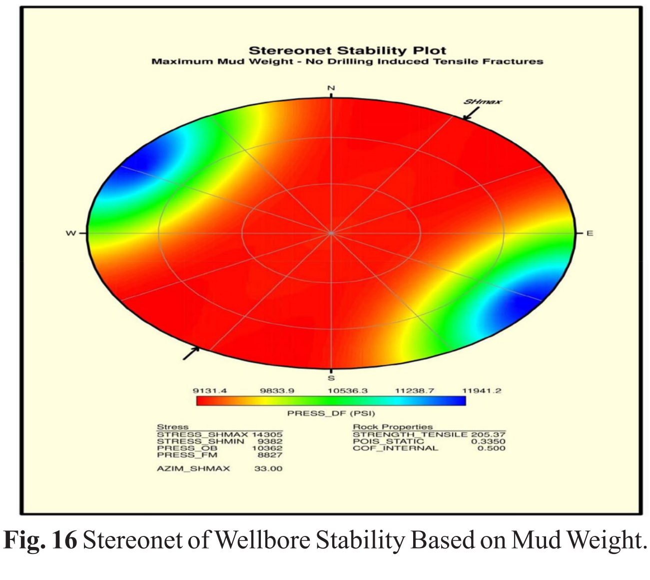

Fig. 16 Stereonet of Wellbore Stability Based on Mud Weight.

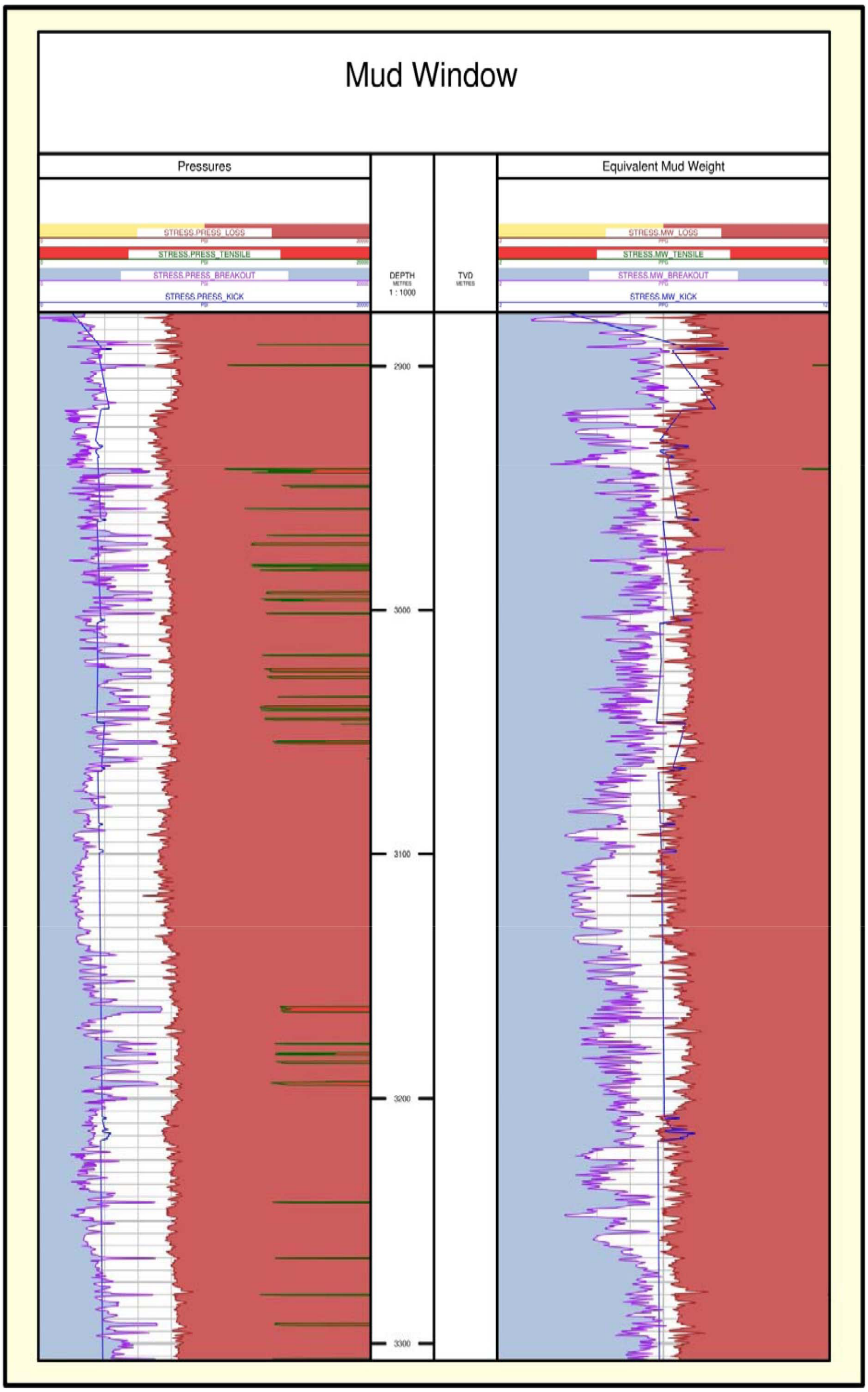

Fig. 17 Appropriate Mud Window for Safe Drilling.

Conclusions

Based on the results, the geomechanical moduli of rock do not change significantly from top to bottom of the depth interval of formation, and it may be considered constant. The maximum amount of anisotropy is on the upper and middle parts of layer 1 and in the middle and lower parts of layer 5. The maximum horizontal stress direction is N33E; most open fractures are in this direction. The minimum horizontal stress direction is in N57W. According to the strongest stability plots, the maximum rock stresses are in SHmax directions, and maximum mud weight is spent in this direction to control and stabilize maximum stress.

Furthermore, directional drilling and oriented perforations should be normal to N33E to cut maximum open fractures. Moreover, the hydraulic fracturing process should be in the direction of N57W to spend minimum energy to produce the deepest and optimized fractures. For continuing directional drilling in the wellbore with minimum sand production, the safe and appropriate mud weight is between 6.5 and 7.5 ppg, which can be considered 7 ppg on average. In the overall interval, with this mud weight and drilling in the normal direction to N33E, problems during drilling related to wellbore instability can be avoided. As a final conclusion, it can be said that DSI permeability and anisotropy results match NMR/SCAL permeability and OBMI-UBI anisotropy results. Therefore, this technique can be applied in the wellbores with no core, NMR, or Image log analysis.

Nomenclatures

UCS: Unconfined Compressive Strength
FZI: Flow Zone Indicator
STC: Slowness Time Coherency
DSI: Dipole Sonic Imager
SCAL: Special Core Analysis
NMR: Nuclear Magnetic Resonance
Shmax: Maximum Horizontal Shear Stress
Shmin: Minimum Horizontal Shear Stress
AZIM-FAST: Fast Azimuth of Shear Wave
DT: Wave Slowness (Sonic Log)
OBMI: Oil-Based Mud Imager Log
UBI: Ultrasonic Borehole Imager Log
K_{st}: Stoneley Permeability ppg Pound per Gallons
N: North
E: East
RHOB: Density Log
IMF: Index Match Factor
K_{ist}: Permeability Index
T_0: Tensile Stress
P_{ob}: Overburden Pressure
P_{for}: Formation Pressure
α: Biot Factor
e_{min}: Minimum Strain
e_{max}: Maximum Strain

References

1. Coates, R., Kane, M., Chang, C., Esmersoy, C., Fukuhara, M., & Yamamoto, H. (2000, November). Single-well sonic imaging: High-definition reservoir cross-sections from horizontal wells. In SPE/CIM International Conference on Horizontal Well Technology. OnePetro, doi.org/10.2118/65457-MS.
2. McLellan, P. J., & Wang, Y. (1994, August). Predicting the effects of pore pressure penetration on the extent of wellbore instability: application of a versatile poro-elastoplastic model, In SPE/ISRM Rock Mechanics in Petroleum Engineering, SPE-28053, SPE, doi.org/10.2118/28053-MS.
3. Aadnøy, B. S., & Hansen, A. K. (2005). Bounds on in-situ stress magnitudes improve wellbore stability analyses, SPE Journal, 10(02), 115-120, doi.org/10.2118/87223-PA .
4. Ezati, M., Azizzadeh, M., Riahi, M. A., Fattahpour, V., & Honarmand, J. (2018). Characterization of micro-fractures in carbonate Sarvak reservoir, using petrophysical and geological data, SW Iran, Journal of Petroleum Science and Engineering, 170, 675-695, doi.org/10.1016/j.petrol.2018.06.058.
5. Ahr, W. M. (2011). Geology of carbonate reservoirs: the identification, description and characterization of hydrocarbon reservoirs in carbonate rocks, John Wiley & Sons.
6. Alawi, R.H., Al-Jawad, M.S. (2021) Wellbore instability management using geomechanical modeling and wellbore stability analysis for Zubair shale formation in Southern Iraq, ournal of Petroleum Exploration and Production Technology, 11, 4047–4062, doi.org/10.1007/s13202-021-01279-y.
7. Alford, R. M. (1986). Shear data in the presence of azimuthal anisotropy: Dilley, Texas. In SEG Technical Program Expanded Abstracts, 476-479, Society of Exploration Geophysicists, doi.org/10.1190/1.1893036.
8. Khoshbakht, F., Azizzadeh, M., Memarian, H., Nourozi, G. H., & Moallemi, S. A. (2012). Comparison of electrical image log with core in a fractured carbonate reservoir, Journal of Petroleum Science and Engineering, 86, 289-296, doi.org/10.1016/j.petrol.2012.03.007.
9. Awal, M. R., Khan, M. S., Mohiuddin, M. A., Abdulraheem, A., & Azeemuddin, M. (2001). A new approach to borehole trajectory optimisation for increased hole stability, In SPE Middle East Oil and Gas Show and Conference, SPE-68092, doi.org/10.2118/68092-MS.
10. Bagheri, H., Tanha, A. A., Doulati Ardejani, F., Heydari-Tajareh, M., & Larki, E. (2021). Geomechanical model and wellbore stability analysis utilizing acoustic impedance and reflection coefficient in a carbonate reservoir, Journal of Petroleum Exploration and Production Technology, 11, 3935-3961., doi.org/10.1007/s13202-021-01291-2.
11. Biot, M. A. (1956). Theory of propagation of elastic waves in a fluid-saturated porous solid. II. Higher frequency range, The Journal of the acoustical Society of america, 28(2), 179-191, doi.org/10.1121/1.1908241.
12. Ma T., Huang J., Jia L., Liu Y., Qiu Y. & Zhang Y. (2020). Wellbore stability analysis for arbitrary inclined well in anisotropic formations, IOP Conference Series: Earth and Environmental Science, 570 062032, doi:10.1088/1755-1315/570/6/062032.
13. Bradley, W. B. (1978, October). Bore hole failure near salt domes, In SPE Annual Fall Technical Conference and Exhibition, OnePetro, doi.org/10.2118/7503-MS.
14. Bradley, W. (1979) Bore Hole Failure Near Salt Domes, paper SPE 7503 presented at the 53th Annual Fall Technical conference and Exibition of the SPE of AIME, 1-3 October, Houston, Texas. doi.org/10.2118/7504-MS.
15. Moos, D., Peska, P., Finkbeiner, T., & Zoback, M. (2003). Comprehensive wellbore stability analysis utilizing quantitative risk assessment, Journal of Petroleum Science and Engineering, 38(3-4), 97-109, doi.org/10.1016/S0920-4105(03)00024-X.
16. Brie, A., Endo, T., Hoyle, D., Codazzi, D., Esmersoy, C., Hsu, K., & Sinha, B. (1998). New directions in sonic logging. Oilfield Review, 10(1), 40-55.
17. Nguyen, V., Abousleiman, Y., Hoang, S. (2007). Analyses of wellbore instability in drilling through chemically active fractured rock formations: Nahr Umr Shale, SPE 105383 presented at the 15th SPE Middle

East Oil & Gas Show and Conference, 11-14 March, Bahrain International Exhibition Centre, Kingdom of Bahrein, doi.org/10.2118/105383-PA.
18. Lee, H., Lee, S.G. & Doyle, P.S. (2015). Photo patterned oil-reservoir micromodels with tailored wetting properties, Lab a Chip 15 (14), 3047–3055, doi:10.1039/C5LC00277J.
19. Liu, H., Cui, S., Meng, Y., Fan, Y., Liu, T., Yu, A., & Hu, Z. (2020). Wellbore stability evaluation method based on the continuous tangent envelope of a Mohr circle. Science Progress, 103(1), 0036850419888465, doi:10.1177/0036850419888465.
20. Simangunsong, R. A., Villatoro, J. J., & Davis, A. K. (2006, September). Wellbore stability assessment for highly inclined wells using limited rock-mechanics data, In SPE Annual Technical Conference and Exhibition?, SPE-99644, doi.org/10.2118/99644-MS.
21. McLean, M. R., & Addis, M. A. (1990). Wellbore stability analysis: a review of current methods of analysis and their field application, In SPE/IADC Drilling Conference and Exhibition, SPE-19941, doi.org/10.2118/19941-MS.
22. Morris, R. L., Grine, D. R., & Arkfeld, T. E. (1964). Using compressional and shear acoustic amplitudes for the location of fractures. Journal of Petroleum Technology, 16(06), 623-632, doi.org/10.2118/723-PA.
23. Santarelli, F. J., Detienne, J. L., & Zundel, J. P. (1989, August). Determination of the mechanical properties of deep reservoir sandstones to assess the likelyhood of sand production, In ISRM International Symposium, Paper Number: ISRM-IS-1989-100.
24. Schlumberger (1997) DSI Dipole Shear Sonic Imager: Corporate brochure SMP-9200, 36.
25. Serra, O. (1989) Formation Micro Scanner Image Interpretation, Schlumberger Education Services.
26. Sibson, R. H. (1996). Structural permeability of fluid-driven fault-fracture meshes, Journal of Structural geology, 18(8), 1031-1042, doi.org/10.1016/0191-8141(96)00032-6.
27. Thiercelin, M. J., & Plumb, R. A. (1994). Core-based prediction of lithologic stress contrasts in East Texas formations, SPE Formation Evaluation, 9(04), 251-258, doi.org/10.2118/21847-PA.
28. Tranggono, H. (2019). Wellbore Collapse Failure Criteria and Drilling Optimization (Master's thesis, University of Stavanger, Norway).
29. Wang, S., Liao, G., Zhang, Z., & Wang, X. (2022). Study on wellbore stability evaluation method of new drilled well in old reservoir, Processes, 10(7), 1334, doi.org/10.3390/pr10071334.
30. Zoback, M. D., Barton, C. A., Brudy, M., Castillo, D. A., Finkbeiner, T., Grollimund, B. R., & Wiprut, D. J. (2003). Determination of stress orientation and magnitude in deep wells, International Journal of Rock Mechanics and Mining Sciences, 40(7-8), 1049-1076, doi.org/10.1016/j.ijrmms.2003.07.001.